Experimental characterization and modeling of the mechanical properties of Cu–Cu thermocompression bonds for three-dimensional integrated circuits

Made, Riko I.; Thompson, Carl V.; Gan, Chee Lip; Yan, Li Ling; Kor, Katherine Hwee Boon; Chia, Hong Ling; Pey, Kin Leong

2012

Made, R. I., Gan, C. L., Yan, L., Kor, K. H. B., Chia, H. L., Pey, K. L., et al. (2012). Experimental characterization and modeling of the mechanical properties of Cu–Cu thermocompression bonds for three-dimensional integrated circuits. Acta Materialia, 60(2), 578–587.

https://hdl.handle.net/10356/96939

https://doi.org/10.1016/j.actamat.2011.09.038

Experimental Characterization and Modeling of the Mechanical Properties of Cu-Cu Thermocompression Bonds for Three Dimensional Integrated Circuits

Riko I Made [a, c, d], Chee Lip Gan [§, a, c], Liling Yan [d], Katherine Hwee Boon Kor [a], Hong Ling Chia [a], Kin Leong Pey [b,c], Carl V. Thompson [c,e]

[a] *School of Materials Science and Engineering*
Nanyang Technological University, 50 Nanyang Avenue 639798 (Singapore)

[b] *School of Electrical and Electronics Engineering*
Nanyang Technological University, 50 Nanyang Avenue 639798 (Singapore)

[c] *Advanced Materials for Micro- and Nano-Systems, Singapore-MIT Alliance,*
4, Engineering Drive 3, Singapore 117576

[d] *Institute of Microelectronics,*
11 Science Park Road, Singapore Science Park II, Singapore 117685

[e] *Department of Materials Science and Engineering, Massachusetts Institute of Technology,*
Cambridge, Massachusetts 02139

[§] *clgan@ntu.edu.sg*

ABSTRACT

An analytical model is proposed which relates the bonding temperature, pressure, and duration with the integrity of metal-metal thermocompression bonds. Unlike previous models, this approach takes into account the pressure-dependent time evolution of the thermocompression bond formation. The model allows calculation of the true contact area of rough surfaces, based

on a creep-dominated plastic deformation. Verification of the model was provided through experiments on Cu-Cu thermocompression bonds of electroplated Cu on diced silicon wafers with chemical-mechanical polished surfaces. The samples were bonded at a range of temperatures, pressures, and times. Shear strength measurements were used to characterize the effects of the bonding parameters on the interface bond strength. Calculated true contact area and bond shear strength can be related by a single proportionality factor. The model can be used to predict the thermocompression bond quality for given bonding parameters and process optimization for reliable bonds, thus assisting in the adoption of the Cu thermocompression bond process in the three-dimensional integrated circuits applications.

Keywords: 3D-IC, Cu-Cu bonds, Thermocompression bonding, True contact area, Shear strength

1. INTRODUCTION

Three-dimensional integrated circuits (3D-ICs) provide an attractive chip architecture that can alleviate interconnect related problems such as signal delay and power dissipation [1,2]. 3D-ICs utilize two or more layers of active electronic components, integrated both vertically and horizontally into a single chip. This 3D approach also facilitates integration of heterogeneous technologies in a single chip [1,3-6].

Apart from monolithic integration [1], bonding of processed wafers or chips is viewed as the cost effective path to achieve 3D-ICs and integration [7]. However, there are still several challenges that must be addressed before this approach can be adopted for mass production. One of the challenges is the communication between active layers. Interactive layer communication is normally achieved using metal-filled holes through the substrate, commonly referred to as through-substrate vias (TSVs) [3,8,9]. Fabrication of TSVs requires etching of high aspect ratio (typically >10:1) vias with uniform diffusion-barrier liners and uniform metal filling. Another problem is the adhesion between layers, which is achieved using dedicated glue materials, direct metal bonding, or a combination of the two [10]. Direct Cu to Cu thermocompression bonding provides the advantage of providing the glue layer for the two active layers as well as the electrical interconnection between the layers.

The quality of direct Cu bonds has been shown to be strongly related to the true contact area [11]. It has been known that micro-roughness of the bond surface results in a true contact area that is significantly less than the nominal contact area. Generally, there are three related

factors that affect the quality of thermocompression bonds. First are the film properties which include surface roughness and surface chemistry. Second is the bonding environment, i.e. the bonding load, temperature and thermal history, vacuum level, and duration of bonding. Third is the instrumentation and control. Empirical relationships between these factors are generally known and have been published [12-14]. However, there is no model available that provides a quantitative understanding that relates all of the bonding parameters to the bond quality. In this paper, an experimental methodology for development of an understanding of the relationship between the bonding parameters is presented. Contact theory is also reviewed, and is utilized as a basis for development of a more general thermocompression bonding model.

2. Contact Area Theory

One of the earliest discussions on contact theory was presented by Hertz [15]. Hertz's contact model allows calculation of the contact area of two spherical bodies that are pressed against each other and which deform elastically. Greenwood and Williamson (GW) [16] expanded this model to take into account the total contact area that is contributed by multiple micro-spherical bodies of asperity that have different heights. GW formulated that when nominally large flat surfaces are pressed against each other, their mean planes become parallel. Thus, by analogy, if a rough surface and a smooth surface are pressed against each other, their mean planes will also become parallel. When the mean plane of the rough surface and the mean plane of the smooth surface are separated by a distance d, summits that have heights $z > d$ will deform. For randomly distributed summit heights, the total number of deformed asperities that form a micro-contact is

$$N_t = A_n \eta \int_d^\infty f(z)\mathrm{d}z\,, \tag{1}$$

where A_n is the nominal contact area, η is the number of asperities per unit area, and $f(z)$ is the asperity height distribution function.

Given that each contacting summit has a height z that exceeds d, the summit must deform by an amount $w = z - d$. Hertz's solution gives the contact area of a fully elastic deforming asperity as

$$A_i = \pi a^2 = \pi R w\,, \tag{2}$$

where a and R are the contact radius and the radius of curvature of the tip of the asperity, respectively, as illustrated in Fig. 1. For multiple asperities, eq. (2) becomes

$$A_c = \eta A_n \pi R \int_d^\infty (z-d) f(z)\mathrm{d}z\,. \tag{3}$$

The load that is supported by the fully elastic deforming asperity is given by [17]

$$L_e = \frac{4}{3} E R^{1/2} w^{3/2} = \frac{4}{3} E R^{1/2} (z-d)^{3/2}\,, \tag{4}$$

where E is the Young's modulus. For multiple asperities, eq. (4) becomes

$$L_{tot-e} = \eta A_n \int_d^\infty \frac{4}{3} E R^{1/2} (z-d)^{3/2} f(z)\mathrm{d}z\,. \tag{5}$$

The GW model accounts for only elastic deformation. However, it has been shown that a small stress concentration on the tip of an asperity could go through plastic deformation [18-20]. Numerous models have been developed to complement GW's model, predicting the plastic component in elastoplastic and fully plastic modes [18,19]. Leong *et al.* [11,21] pointed out

that certain materials also experience work hardening effects. Their model is based on the model of Chang *et al.* which accounts for volume conservation. For plastically dominated asperity deformation, the total true contact area of a microscopically rough surface can be represented as

$$A_i = \pi a^2 = 2\pi R w, \tag{6}$$

which modifies eq. (3) into

$$A_c = 2\eta A_n \pi R \int_d^{\infty} (z-d) f(z) \mathrm{d}z . \tag{7}$$

Apart from the extent of elastic and plastic deformation, all of the aforementioned models consider only the behavior of asperity deformation at a single temperature. Thus, the model do not predict the true contact area across different temperatures. However, it is known that plastic deformation is a temperature-dependent dynamic process. Hill and Wallach [22] considered the time and temperature effects in their modeling of Cu-Cu bonding. However, their model is oversimplified in several ways. First, the surface roughness geometry is modeled as parallel ridges that are formed by a two dimensional array of semi cylinder. Contacts are formed at the peaks of the ridges. All of the ridges were assumed to have the same height and the peaks were evenly spaced. However, real surfaces have a random distribution of peaks and valleys. Second, they assumed that the deformation was fully plastic, with no elastic component, from the beginning of the bonding process. This leads to over-prediction of true contact area.

In this paper, a model for prediction of the bond quality given the bonding conditions, i.e. the bond temperature, pressure, time, and surface roughness, is developed. In addition, a simple bonding experiment was conducted to determine the proportionality factor that relates the model's prediction and the actual bond's mechanical properties.

3. Modeling of True Contact Area Formation

The dynamic nature of contact as a function of time is illustrated in Fig. 1. Under a constant load, asperities that are in contact deform continuously, which results in a decrease in the mean plane distance d. From eq. (1), the number of asperities in contact increases as d decreases, which has the consequence of increasing the true contact area as described by eq. (7). Thus, d is now replaced by $d(t)$ to show the time dependence of the mean plane distance.

The contacting asperity is now considered as having a linear viscoelastic behavior, where the asperity deformation function can be separated into both creep response and load. A single asperity in contact is modeled as a Kelvin-Voigt material that can be represented by a pure viscous *damper* and a purely elastic *spring* connected in parallel as shown in Fig. 2 [23]. Any deformation represented by the damper component is assumed to be irreversible. Under normal loading, the total average stress on the contacting asperity will be the sum of each component expressed as

$$p_{tot} = p_e + p_r, \tag{8}$$

where p_e is the elastic component of the compressive stress and p_r is the relaxation stress contributed by the action of creep. Here, p_e is simply taken as $p_e = L_e / A_i$, where L_e and A_i have been defined in eq. (4) and eq. (6), respectively. The stress relaxation component p_r can be expressed as

$$p_r = -\int E\dot{\varepsilon}(p,T)\mathrm{d}t, \tag{9}$$

which describes the amount of stress that is relaxed by plastic deformation at a particular temperature T. $\dot{\varepsilon}(p,T)$ is the plastic strain rate of the active deformation mechanism(s) and is both pressure and temperature dependent. $\dot{\varepsilon}$ is given a negative value, as the deformation rate is decreasing over time.

Similarly, L_e and L_r represent the elastic load and relaxation load component, respectively. Multiplying eq. (8) by the asperity true contact area A_i, the load that is being held by each single asperity can be expressed as

$$\begin{aligned} L_i &= L_e + L_r \\ &= (4/3)ER^{1/2}w^{3/2} - A_i\int E\dot{\varepsilon}(p,T)\mathrm{d}t \\ &= (4/3)ER^{1/2}w^{3/2} - 2\pi Rw\int E\dot{\varepsilon}(p,T)\mathrm{d}t \\ &= (4/3)ER^{1/2}(z-d(t))^{3/2} - 2\pi R(z-d(t))\int E\dot{\varepsilon}(p,T)\mathrm{d}t \end{aligned} \tag{10}$$

where A_i is obtained from eq. (6) to take into account volume conservation. Integrating eq. (10) over the entire possible range of values, i.e. from d to ∞, we have

$$L_{tot} = A_n\eta E\left((4/3)R^{1/2}\int_{d(t)}^{\infty}(z-d(t))^{3/2}f(z)\mathrm{d}z - 2\pi\int_{d(t)}^{\infty}\int_{0}^{t}\dot{\varepsilon}(p,T)\cdot R\cdot(z-d(t))f(z)\mathrm{d}t\mathrm{d}z\right), \tag{11}$$

with L_{tot} typically held constant during the thermocompression bonding process.

Thermocompression bonding is typically carried out in a temperature range from 200 ℃ (~0.3T_m of Cu) to 400 ℃ (~0.5T_m). In that range, material deformation is dominated by power-law creep. Deformation that is governed by power-law creep can be described by [24]

$$\dot{\varepsilon} = H_c\frac{D_{eff}\mu b}{kT}\left(\frac{\sigma}{\mu}\right)^n, \tag{12}$$

where H_c is the Dorn constant, μ is the shear modulus, b is the Burger's vector, σ is the applied stress, k is Boltzmann's constant, T is the temperature, and n is the stress exponent and has a value between 3 and 10 [24]. The effective diffusivity, D_{eff} is given by [25]

$$D_{eff} = D_v\left[1+\frac{10a_c}{b^2}\left(\frac{\sigma}{\mu}\right)^2\frac{D_c}{D_v}\right], \tag{13}$$

where a_c is the dislocation core diameter, D_v and D_c are the lattice and dislocation core diffusivity, respectively. The Dorn constant H_c has been shown to be dependent on the stress exponent. In face-centered cubic metals, the relationship between these quantities can be expressed as [26]:

$$\log_{10} H_c = 2.94(n-2.95). \tag{14}$$

Grain-boundary diffusion and power-law creep were considered by Keller *et al.* [27] as the two possible relaxation mechanisms. Gibbs [28] has described grain-boundary diffusion deformation in thin films as

$$\dot{\varepsilon} = A_g\frac{\Omega\sigma}{kTd_g h^2}\delta D_g, \tag{14}$$

where A_g is a constant, Ω is the atomic volume, d_g is the grain size, h is the film thickness, δ is the grain boundary width, and D_g is the grain-boundary diffusivity, and is given as

$$D_g = D_{og}\exp(-Q_g/kT), \tag{16}$$

where D_{og} is a constant and Q_g is the activation energy for grain-boundary diffusion.

4. Simulation Results

The two possible stress relaxation mechanisms described above were considered and simulated. The true contact area was estimated based on the surface morphology using eq. (7), where the input value for the mean plane spacing d was determined arithmetically such that eq. (11) is satisfied. With L_{tot} assumed to be constant during the thermocompression bonding process, a suitable value of d can be chosen to satisfy eq. (11) for each given bonding condition. Table 1 lists all the constants that were used in the calculations. After obtaining d, the true contact area can be calculated based on eq. (7).

Table 1. List of physical constants for creep dominated asperity deformation

Symbol	Magnitude	Reference
E	128 GPa	
ν	0.34	
A_g	12	[27]
Ω	1.18×10^{-29} m^3	[24]
δD_{og}	5×10^{-15} m^3/s	[24]
Q_g	104 kJ/mol	[24]
H_c	7.4×10^{-5}	[24]
μ	4.21×10^{4} MPa	[24]
b	2.56×10^{-10} m	[24]
n	4.8	[24]
$a_c D_{oc}$	1×10^{-24} m^4/s	[24]
Q_c	117 kJ/mol	[24]

D_{ov}	2×10^{-5} m^2/s	[24]
Q_v	119 kJ/mol	[24]

Fig. 3(a) shows the simulation results based on stress relaxation by grain boundary diffusion dominated creep. The simulation was conducted by assuming that a chemical-mechanical-polished (CMP) Cu surface has a surface roughness parameter σ = 3 nm, an average asperity radius of curvature $\overline{R}$ = 50 nm, an asperity density $\eta = 10^{14}$ m^{-2} [21] and an average grain size d_{gb} = 400 nm. The simulation results show that the true contact area has very strong and unrealistic time dependence. A perfect bond interface (i.e. 100% true contact area) can be achieved at very short bonding times. At bonding temperatures of 200 ℃ and 400 ℃, complete bonding can be achieved in 33.9 μs and 0.06 μs, respectively, even at a relatively low bonding pressure of 100 kPa. This result does not correlate well with observations from actual bonding. In general, a temperature above 300°C and 30 min bond duration is necessary to achieve a reliable bond quality [29]. These results also do not correlate well with experimental results from [30]. It is clear from this simulation that thermocompression bonding is unlikely to be governed by grain boundary dominated diffusion creep.

Fig. 3(b) shows the simulation results based on power law creep dominated deformation. The simulation results show a slower evolution of the true contact area. A very fast increase happens at the beginning of the bonding process, but the rate decreases at longer times. No significant improvement in the bond integrity with an increase in the bond duration at low bonding temperatures (below 300°C) is observed. On the other hand, simulations at higher bonding temperatures (above 300°C) show that the true contact area growth saturates at a much

later time as compared to bonding at a lower temperature (below 300°C). This implies that bond integrity will benefit from longer bonding times if the bonding temperature is high enough. Conversely, there may not be much benefit of long bond times if the bonding temperature is low.

The simulation results are also consistent with the experimental results shown by Leong *et al.* [21]. Leong observed that at least 3.18×10^{-2} % true contact area is required to obtain 100% dicing yield. This observation was based on bonding of CMP finished, 200 mm diameter blanket Cu wafers, at a 8 kN bonding load (254.8 kPa) for 30 mins (1800 s) at 300°C. Even though the results were only simulated up to 1000 s, a rough extrapolation of the simulation results suggests that the predicted true contact area is close to 3.18×10^{-2} % for the simulation at 300°C. Based on Leong's criteria, it can also be argued that a bonding pressure of 100 kPa and a bonding temperature of 250°C or lower will result in less than a 100% dicing yield. In practice, higher yield is always desired. With the current model, the bonding condition required to achieve the maximum bonding yield can be estimated.

The simulation results were also compared against experimental data from Nichting [30], as shown in Fig. 4. To simplify the comparison, it is assumed that the experimentally measurable mechanical strength of the bonded chip can be related to the calculated true contact area by a single constant. Nichting's results also showed that the bond integrity improved quickly at the early stage of bonding. Bond integrity improvement was also observed to reduce with longer bonding times, particularly at low bonding temperatures. A point to note is that the mechanical properties of an asperity could be different from bulk Cu due to its size effect, which will affect the model's prediction. Nevertheless, the trends given by the model would still be consistent with the experimental data. Overall, the simulations that are supported by the experimental results in

[30] strongly suggest that the Cu-Cu thermocompression process is governed by power law creep deformation.

The simulation results predict the true contact area from the bonding process, which can be related to the bond integrity through a single proportional factor K [31], given as

$$F = K \times A_c, \tag{17}$$

where A_c is the calculated true contact area from eq. (7) and F is the predicted shear force in shear testing. The true contact areas were calculated based on Nichting's [30] sample's surface roughness and bonding conditions. The root-mean-square (rms) surface roughness and other parameters such as the radius of curvature R, asperity density η and asperity height distributions $f(z)$ were taken or interpolated from Leong's data [21]. The proportionality factor K is obtained by re-plotting all the experimental data from Nichting *et al*. [30] as a function of the calculated true contact area, as shown in Fig. 5. K is the slope of the best fitting curve and it is assumed to be valid across different bonding temperatures. K was found to be 606.7 ± 35.8 MPa. The current model for the experimental fittings assumes that the proportionality factor K is the same for shear and pull tests of Nichting *et al*. [30], which may be incorrect. A point to note is that the value of K determined here is within the same order of magnitude as the bulk Cu shear strength (172 MPa) (ASTM B370-09). To determine whether it is reasonable take to K be the shear strength and determine the actual value of K, experiments were conducted.

5. Experiments

To test the model, the shear strength of thermocompression bonded Cu samples was collected for different bonding conditions. Copper was deposited on silicon chips with two different sizes (5×5 mm^2 and 2.5×2.5 mm^2) and the chips were bonded face to face. Three pairs of chips were bonded in each bonding cycle carried out at different conditions. Bonded chips were then subjected to shear testing to measure the bond toughness.

The Cu films were deposited on a 200 nm-thick SiO_2 film that was grown on silicon wafers using plasma enhanced chemical vapor deposition (PECVD) at 300°C. A 250 Å-thick Ta layer was used as an adhesion layer under the Cu. The 1 μm thick Cu layer was deposited using an electrochemical plating (ECP) process in which Cu seed layers (150 nm) were deposited using physical vapor deposition (PVD). An N_2 anneal at 200°C for 30 minutes was carried out prior to Cu CMP, to reduce the Cu thickness to about 400 nm.

Prior to the bonding, the surface roughness of the diced chips was characterized using atomic force microscopy (AFM). The surface roughness parameters $\overline{R}$, σ and η were then estimated using an algorithm developed by Leong *et al*. in [21].

As the presence of Cu oxide on the sample surface is detrimental to the bond quality [11,29,32], both chips were dipped in acetic acid for 10 minutes to remove the surface oxide and subsequently blown dry with a nitrogen airgun prior to in a bonding in a vacuum [11]. The samples were bonded face to face with three pairs of chips bonded in each bonding cycle. The three pairs were positioned in a way that allowed the load to be distributed evenly, that is,

the samples were radially distributed with a 120° separation from the nearest neighbors. A customized fixture was designed to allow easy placement of the bonding pairs.

All of the samples were bonded in a 10^{-2} Torr ambient environment, with the total bonding load for the three samples being 400 g (209.1 kPa/chip), 1200 g (627.2 kPa/chip) and 2400 g (1254.4 kPa/chip) for different durations (70, 240 and 700 minutes), and with a temperature range of 200°C - 400°C.

To characterize the bond quality, chip shear testing was carried out using a DAGE 4000 Multi-purpose Bondtester™. The bonded samples were put on the stage in such a way that the bottom chip was being held by a metal stopper, while the top (smaller) chip was pushed parallel to the sample surface. The blade travelled with a constant velocity of 50 μm/s until fracture was detected as a sudden drop in applied force. The maximum force required before fracture was recorded. To avoid friction between the shearing blade and the bottom chip, the tip of the blade was placed 5 μm above the bottom chip's surface.

6. Results and Discussion

At the end of section 4, we made an assumption that K could be taken to be the bulk Cu shear strength, due to the relatively close value of K obtained from Nichting *et al*. [30]. Fig. 6 shows the experimental bond strength results for chip-to-chip bonding, superimposed with the model prediction. Simulation results were compared to the experimental results by assuming a proportionality constant of 172 MPa, which is the bulk Cu shear strength.

At 70 mins bonding time (Fig. 6 (a)-(c)), the model predictions are close to the mean value of the measured shear strength for the entire bonding pressure range. At medium (240 mins) bonding times (Fig. 6(d)-(f)), the model predictions are close to the experimental results up to 300°C. At higher temperatures, the model generally under predicts the bond strength. Scattered measurement results obscure any transition point. For a longer bond duration of 700 mins, at lower bonding loads, a good correlation between the model and measured values is observed up to 300°C (Fig. 6(g)-(h)). However, for a high bonding load and long bonding time, as shown in Fig. 6(i), the model completely under predicts the bond strength.

There are a few possible explanations for these discrepancies between the model predictions and the experimental results at high pressures and long bonding times. These include the possibility that the exponential factor n varies or that an unsuitable K value was used. Discrepancy due to the presence of a copper oxide can be ruled out as the presence of an oxide on the interface is generally regarded to be detrimental to the bond quality, so that the model should over-predict the bond strength [33]. On the other hand, it is known that the stress exponential factor in eq. (12) can vary from $n = 3$ to $n = 10$ in a temperature range from $0.3T_m$ to $0.5T_m$ and at higher applied stress [24].

Further simulations with different values of n generally give a better fit to the experimental results, with the simulation with $n = 10$ giving a better prediction up to 300°C, though the model becomes unrealistic when the temperature exceeds this value (results not shown). Generally, a higher stress exponential factor up to $n = 9$ gives a better fit to the experimental results in Fig. 6(i). However, the model is still under-predicts the experimental values. Changes in the stress exponential factor could be attributed to a change in the

deformation mechanism. Under the same power law regime, dislocations could gain an extra degree of freedom, such as a combination of dislocation climb and dislocation glide [24]. Thus, different n values at different stress levels are possible.

Even though a higher n gives a better fit to the data, the absolute values of the model prediction are still lower than the experimental results. Thus, K is empirically determined by re-plotting all the experimental data as a function of the calculated true contact area, as shown in Fig. 7. It is observed that data from the die shear test has a wider distribution, as compared to the pull test data shown in Fig. 5. This may be inherent to this characterization method, as pull test is known to result in less data scattering as compared to die shear test [34]. K is the slope of the best fitting curve and it is assumed to be valid across different bond temperatures and pressures. K was found to be 405.5 ± 52.3 MPa, within the same order of magnitude of the bulk Cu shear strength. However, it still under-predicts the experimental results at high bonding temperature and bonding pressure (Fig. 6 (i)). Furthermore, the fits become worse (over-prediction) for experimental results at lower bonding pressure (Fig. 6 (a), (d) and (g)).

An alternative to the empirical determination of a single constant *K*, different values of K can be empirically determined for different bonding regimes. A similar approach as discussed in section 4 was used, with K determined from the slope of measured bond shear strength versus A_c, for different bond times and pressures as shown in Fig. 8. It was found that K has a range between 47 MPa to 2800 MPa, with a higher K observed at higher bonding pressures. K ranges from 47 MPa to 200 MPa, 240 MPa to 510 MPa, and 1100 MPa to 2800 MPa at 209.1 kPa, 627.2 kPa and 1254.4 kPa bonding load, respectively. The observation that relatively similar K values at the same bonding load suggests that K could be a function of bond pressure.

The apparent pressure dependence of K might be related to various shielding (energy-absorbing) effects from mechanical testing, i.e. fracture modes changes, plastic energy dissipation, crack propagation path, geometry of test sample, etc. [35]. By using shear test in this work, it is assumed indirectly that the crack would follow the bond interface line. This assumption is valid for samples bonded at shorter bonding duration and lower bond pressure, where analysis of the failed interface showed that the crack due to the shear test indeed followed the bond interface. These bonding conditions correspond to a low true contact area, which gave a better fit between the simulation results and the experiments data. However, this may not be true for all bonding conditions. At higher bond pressures, which are associated with higher true contact areas, the failure path may not be confined to the bond interface, which may give an apparently higher true contact area, and hence measured higher bond strength.

Wenning and Müser [36] have suggested that K is not a constant, but varies with pressure. On the other hand, Mo *et al*. [37] argued that an asperity contact A_c consists of yet smaller contacts (A_{real}), which have smaller length scales than the asperity length scale. At high contact force, A_{real} could approach A_c , so that the relationship between asperity contact and shear force becomes linear, i.e. K becomes a constant. At this time, there is no way to determine A_{real} and the pressure dependence of K .

Despite the discrepancies in details discussed above, the current model, which consistently underestimates the experimental bond strength, can provide practical guidance for the bonding process. The model can also be seen as an advancement from the previous model by Leong [11], as the current model includes bonding temperature and bonding time as components for predictions, which were not considered in the previous model.

7. Bonding Maps

From the point of view of manufacturing, wafer bonding should be performed at a temperature that is reasonably low, for a time that is as short as possible. A one hour bonding time with a bond pressure ranging between 200 kPa and 10 MPa [38], at a temperature between 200 ℃ and 400 ℃, is typically considered to be reasonable.

Leong *et al.* [11] showed a correlation between the theoretical true contact area and the dicing yield for wafers that were bonded at 300 ℃. An approximate true contact area of 1×10^{-5} m^2 or above is required for a 100% dicing yield for bonding 8" diameter Si wafers coated with 400 nm-thick blanket Cu films. Similarly, a 3×10^{-6} m^2 area is the threshold for zero dicing yield. Normalized with respect to the wafer area, the boundary condition for 100 % dicing yield and zero threshold dicing yield will be 3.18×10^{-4} and 9.55×10^{-6}, respectively. The normalization was based on the assumption that the bonding is uniform across the bonding surfaces, which can be considered reasonable for blanket wafers. Leong also suggested that the results can be generalized for bonding of either 6" or 12" wafers, as long as the bond pressure is kept constant.

Bonding maps that take into consideration of the bond temperature can be constructed based on the same criteria as those used by Leong *et al*, and using the new model. Fig. 9 shows a bonding map that includes bond pressure and temperature for various surface roughnesses. From the maps, one can estimate a 100% dicing yield will be achieved if the bonding conditions falls above the 3.18×10^{-4}curve. On the other hand, wafers dicing will have zero yield if the bonding condition falls below the 9.55×10^{-6} curve. The map assumes a one hour bonding time [39] at a

bond pressure ranging from 10 kPa to 10 MPa, a bonding temperature ranging from 200 ℃ to 400 ℃, and a surface roughness ranging from 1 nm to 5 nm-rms, which is currently achievable by industry using CMP. Low bond pressures around 10 kPa would be useful for integration involving low-k materials, which are known to be mechanically weak [40,41].

Overall, the maps show little variation with respect to varying surface roughness from 1 to 5 nm-rms. The small variation is good for manufacturing as surface roughness is relatively difficult to control compared to other bonding condition. Low variations also give larger tolerance in processing conditions. Furthermore, surface roughness of 1 to 5 nm-rms is easily achieved in the CMP process. Variation in the true contact area due to the surface roughness decreases as the bond pressure increases. This implies that the effect of surface roughness on the true contact area can be virtually eliminated with high pressure bonding.

The use of high bonding pressures also allows bonding at lower temperatures. For example, a bonding temperature of 350 ℃ is required to achieve 1% true contact at 2 MPa, while the same true contact area can be achieved at 200 ℃ with a 10 MPa bond pressure. While this prediction is important, we were unable to test it due to limitations of our bonding equipment.

Summary and Conclusions

A model that provides a quantitative estimate of the true contact area that can be achieved as a function of surface topographic characteristics and the applied load, as well as temperature and bonding time has been developed and tested. Creep dominated deformation of surface

asperities affects the time and temperature dependence of the true contact area. Both grain boundary creep and power law creep were considered and simulated. Only power law creep led to a prediction of realistic results that were in line with experimental reports. Simulations based on the model were found to fit experimental results for chip-to-chip bonding reasonably well, underestimating bond strengths in those cases in which the disagreement between the model and experiments were greatest. A proportional constant K was used to correlate the model prediction of the true contact area with measured bond shear strengths. K was empirically determined and was found to have a dependence on the bonding pressure.

The model can be used as a predictive tool for practical applications. A map relating predicted true contact areas to surface roughness and bonding conditions have been developed. This map provides a tool for process optimization for high-quality bonds.

8. Acknowledgements

The authors acknowledge the Singapore MIT Alliance, which made the current work possible. R. I Made also particularly acknowledges Mr Wardhana Aji Sasangka from the Singapore MIT Alliance for designing the chip bonder.

References

[1] R. Chanchani, in *Materials for Advanced Packaging* (2009), pp. 1-50.
[2] K. C. Saraswat, K. Banerjee, A. R. Joshi, P. Kalavade, P. Kapur, and S. J. Souri, In: Proceedings of the 26th European Solid-State Circuits Conference, ESSCIRC'00. 2000. p.406-414 .
[3] P. Ramm, A. Klumpp, R. Merkel, J. Weber, R. Wieland, A. Ostmann, and J. Wolf, in *Materials Research Society Symposium Proceedings* (2003), pp. 3–14.
[4] W. Weber, in *Materials Research Society Symposium Proceedings* (2007), p. 103.
[5] J. Lu, T. Cale, and R. Gutmann, in *Materials for Information Technology* (2005), p. 405-417.

[6] K. Lee, T. Fukushima, T. Tanaka, and M. Koyanagi, in (Las Vegas, NV, 2010), p. 71-90.
[7] A. W. Topol, J. D. C. La Tulipe, L. Shi, D. J. Frank, K. Bernstein, S. E. Steen, A. Kumar, G. U. Singco, A. M. Young, K. W. Guarini, and M. Ieong, IBM Journal of Research and Development **50**, 491 (2006).
[8] M. Bonkhara, In Conference on 3D Architecture for Semiconductors and Packaging , Burlingame, *CA* (2004).
[9] R. Hon, S. W. R. Lee, S. X. Zhang, and C. K. Wong, in Proceedings of 7th Electronic Packaging Technology Conference, 2005; 2005. (2005). p. 6
[10] J. Q. Lu, J. J. McMahon, and R. J. Gutmann, (n.d.).
[11] H. L. Leong, C. L. Gan, C. V. Thompson, K. L. Pey, and H. Y. Li, J. Appl. Phys. **102**, 103510
[12] T. Suga, In: *Proceedings. 50th Electronic Components and Technology Conference, 2000.* p. 702-705.
[13] C. H. Tsau, S. M. Spearing, and M. A. Schmidt, Microelectromechanical Systems, Journal Of 2004;**13**, 963-971.
[14] T. Suga, *Semiconductor Wafer Bonding 10: Science, Technology, and Applications* (The Electrochemical Society, 2008).
[15] H. Hertz and J. R. Angew, *Translated and Reprinted in English as Hertz's Miscellaneous Paper* Macmillan; 1986.
[16] J. A. Greenwood and J. B. P. Williamson, Proceedings of the Royal Society of London. Series A, Mathematical and Physical Sciences 1966;**295**, 300-319 .
[17] J. I. McCool, Wear 1986;**107**, 37-60 .
[18] W. R. Chang, I. Etsion, and D. B. Bogy, J. Tribol. 1987;**109**, 257-263 .
[19] L. Kogut and I. Etsion, J. Appl. Mech.2002; **69**, 657-662 .
[20] A. H. Uppal and S. D. Probert, Wear 1973;**23**, 173-184 .
[21] H. L. Leong, Quantitative Analysis of the Mechanical and Electrical Properties of Cu-Cu Bonds for Three-dimensional Integrated Circuits (3D ICs)., Singapore MIT Alliance, Nanyang Technological University, 2007.
[22] A. Hill and E. R. Wallach, Acta Metall1989; **37**, 2425-2437 .
[23] M. A. Meyers and K. K. Chawla, *Mechanical Behavior of Materials* (Prentice Hall New York, 1998).
[24] H. J. Frost, *Deformation-Mechanism Maps: The Plasticity and Creep of Metals and Ceramics* (Pergamon Press, 1982).
[25] R.-M. Keller, S.P Baker, and E. Arzt, J. Mater. Res. 1998;**13**, 1307 .
[26] A. M. Brown and M. F. Ashby, Scr. Metall 1980;**14**, 1297-1302 .
[27] R.-M. Keller, S. P. Baker, and E. Arzt, Acta Mater. 1999;**47**, 415-426 .
[28] G. B. Gibbs, Philosophical Magazine **13**, 1966;589-593 .
[29] K. Chen, C. Tan, A. Fan, and R. Reif, Journal of Electronic Materials **34**, 1464-1467 (2005).
[30] R. Nichting, D. Olson, and G. Edwards, Journal of Materials Engineering and Performance 1992;**1**, 35-44 .
[31] J. Krim, Langmuir 1996;**12**, 4564-4566 .
[32] H. L. Leong, C. L. Gan, R. I. Made, C. V. Thompson, K. L. Pey, and H. Y. Li, J. Appl. Phys. 2009;**105**, 033514-6 .
[33] H. A. Francis, ASME J. Eng. Mater. Tech 1976;**98**.
[34] O. Vallin, K. Jonsson, and U. Lindberg, Materials Science and Engineering: R Rep2005; **50:** 109-165 .
[35] M. Lane, Annu. Rev. Mater. Res.2003, **33**, 29-54 .
[36] L. Wenning and M. H. Müser, Europhys. Lett. 2001;**54**: 693-699 .
[37] Y. Mo, K. T. Turner, and I. Szlufarska, Nature 2009;**457**, 1116-1119 .
[38] T. Suga, ECS Trans 2006;**6**, 155-163.
[39] K. Chen, A. Fan, C. Tan, and R. Reif, Journal of Electronic Materials 2006;**35**, 230-234 .

[40] A. A. Volinsky, J. B. Vella, and W. W. Gerberich, Thin Solid Films 2003;**429**, 201-210 .
[41] J. B. Vella, I. S. Adhihetty, K. Junker, and A. A. Volinsky, International Journal of Fracture 2003;**120**, 487-499 .

Figures

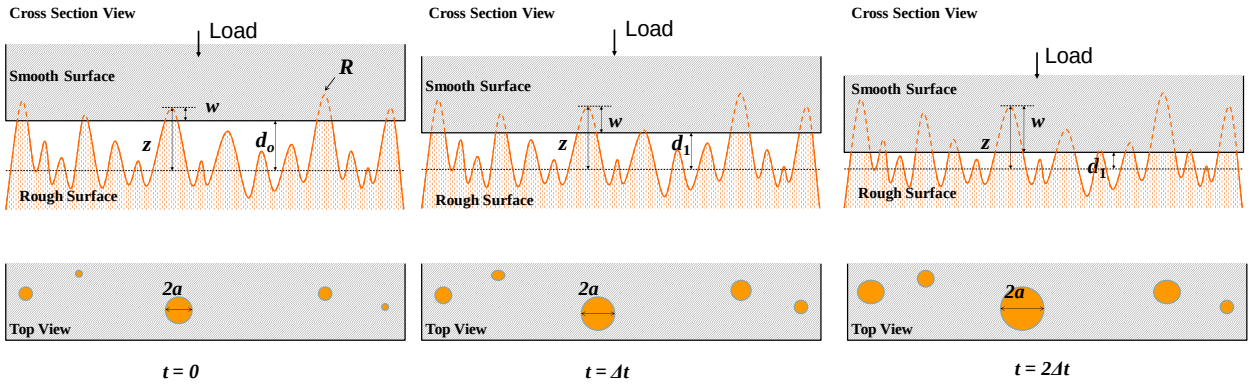

Fig. 1 Summits that have heights $z > d$ will deform by an amount $w = z - d$. With the contribution of creep, d will decrease over time as the asperities are subjected to plastic flow, resulting in more asperities making contact and increasing the total true contact area.

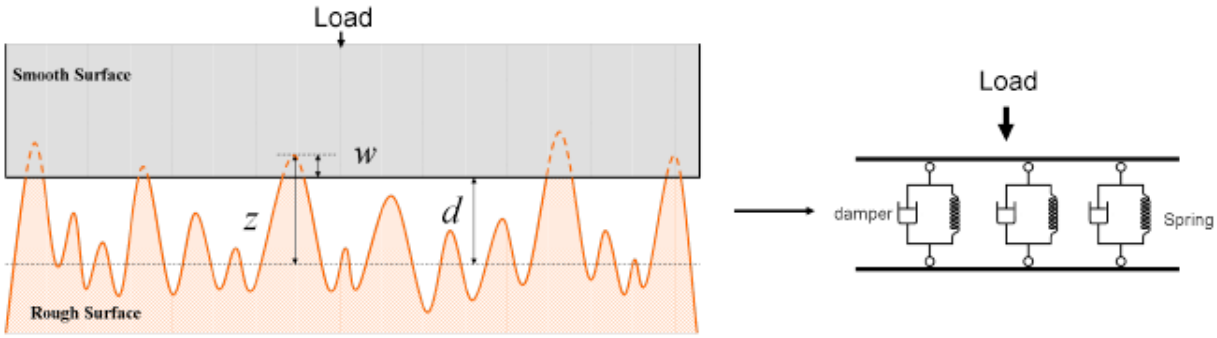

Fig. 2 A single asperity contact is modeled as a Kelvin-Voigt material that can be represented by a pure viscous damper and a purely elastic spring connected in parallel.

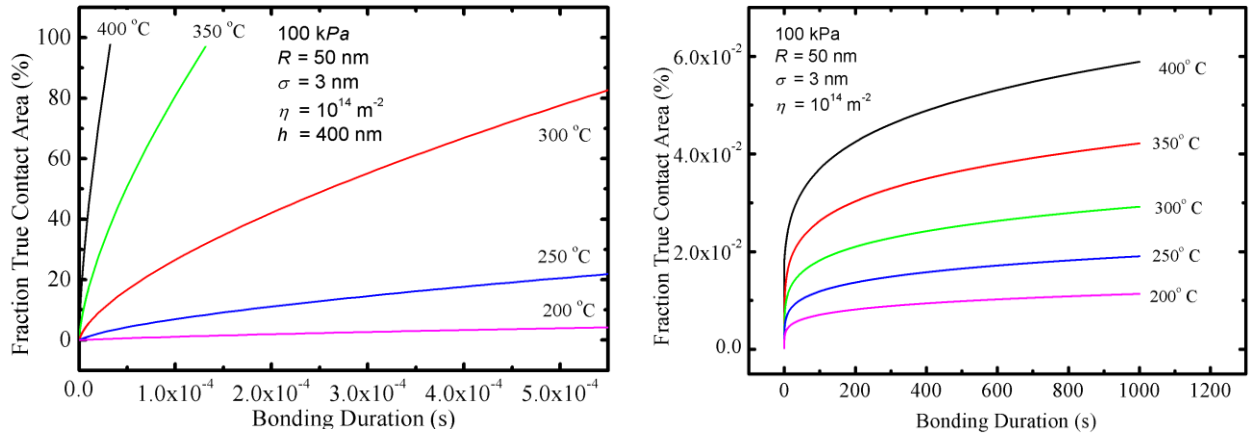

(a) (b)

Fig. 3 Simulated true contact areas for different creep mechanisms, (a) grain-boundary diffusion creep-dominated deformation; (b) power law creep-dominated deformation. The power-low creep- mechanism shows better agreement with the experiments of Nichting [30].

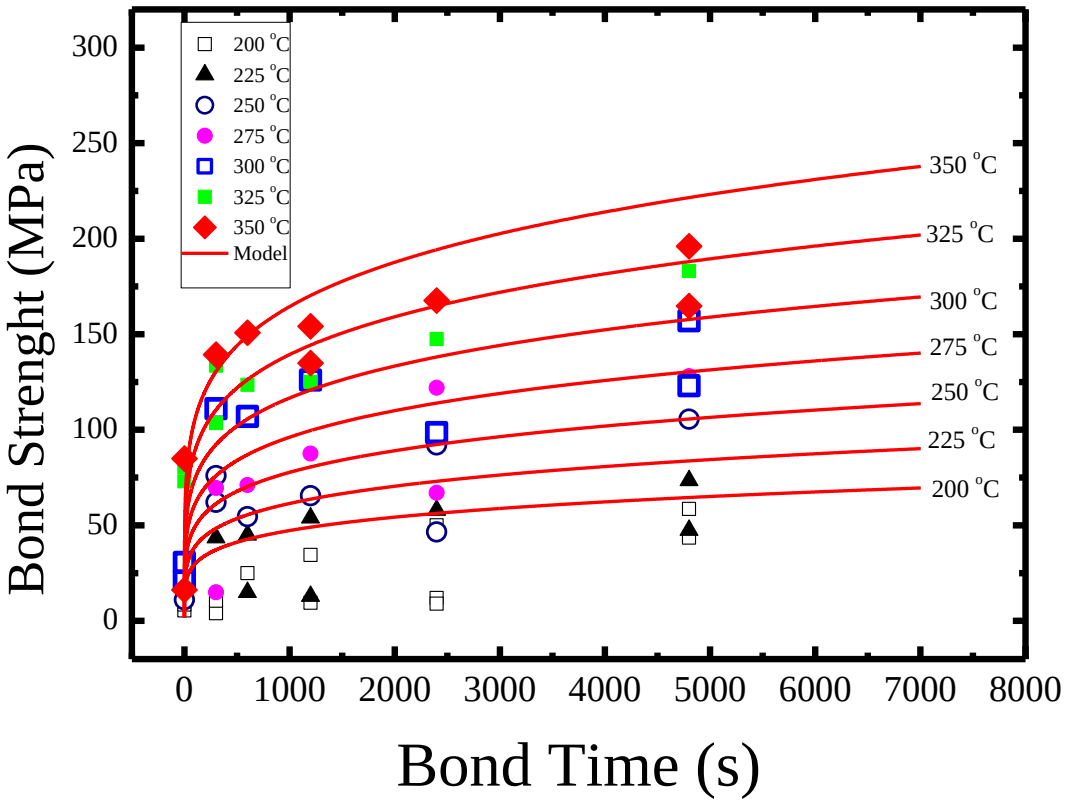

Fig. 4 Cu bond toughness determined using the pull test method, extracted from the experimental results of Nichting [30].

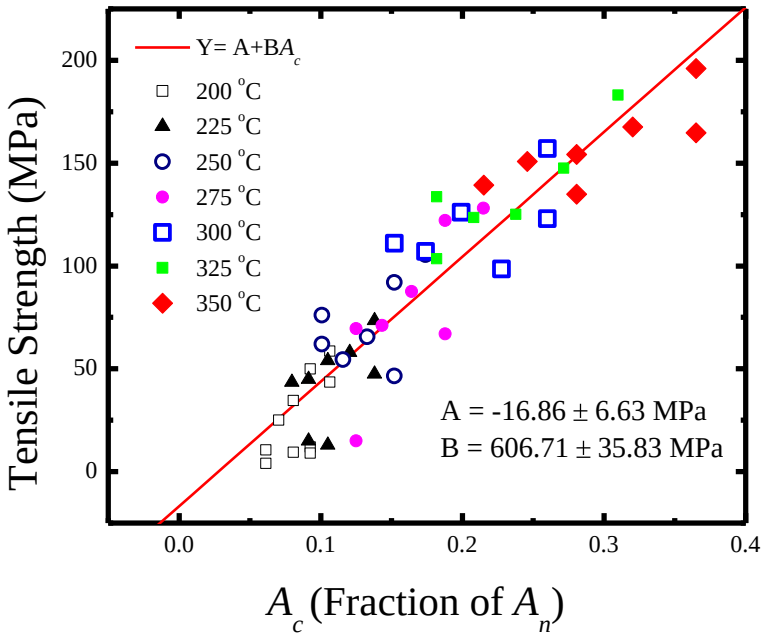

Fig. 5 Measured bond strengths from Nichting et al. [30] plotted versus the calculated true contact area. K is the slope of the best-fit line.

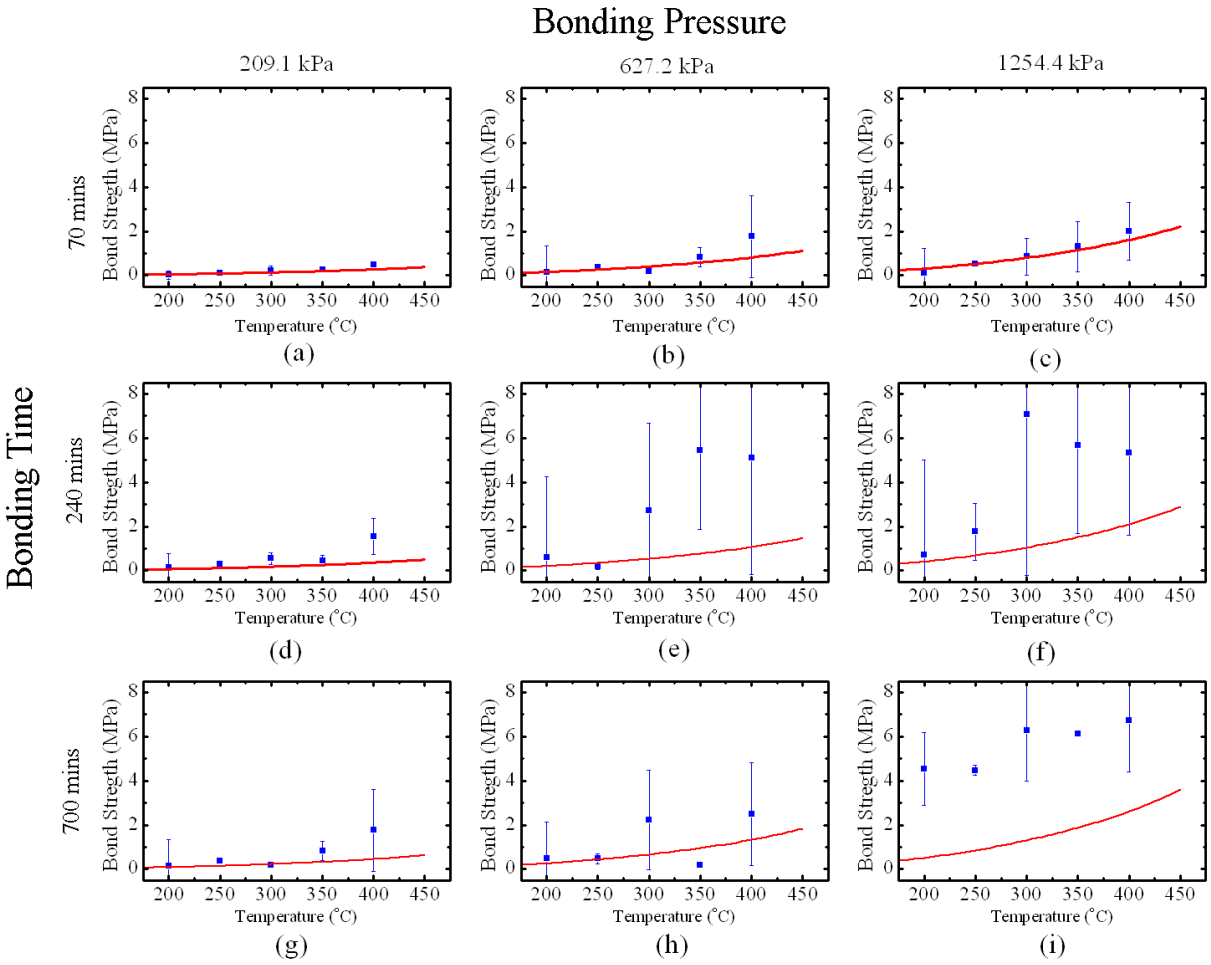

Fig. 6 Experimental results for chip-to-chip bonding, superimposed with model predictions. The solid lines represent model predictions which are related to the experimental results by a factor of 172 MPa (K). The model was simulated with stress exponential factor n = 4.8 [27].

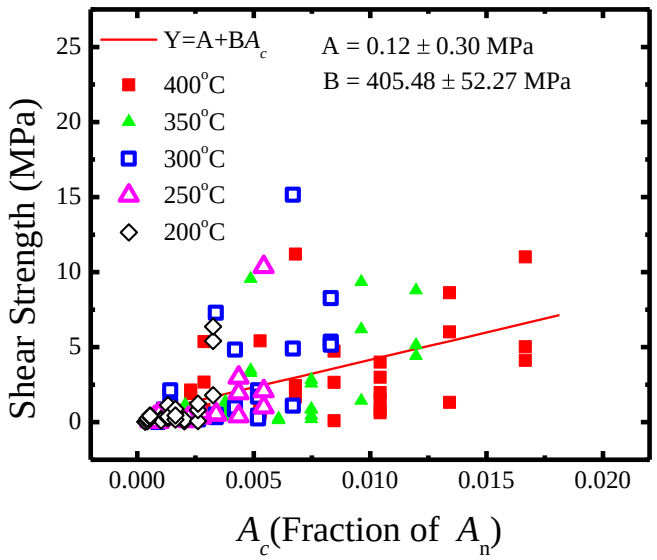

Fig. 7 Measured bond strengths from shear tests plotted versus the calculated true contact area. K is the slope of the best-fit line.

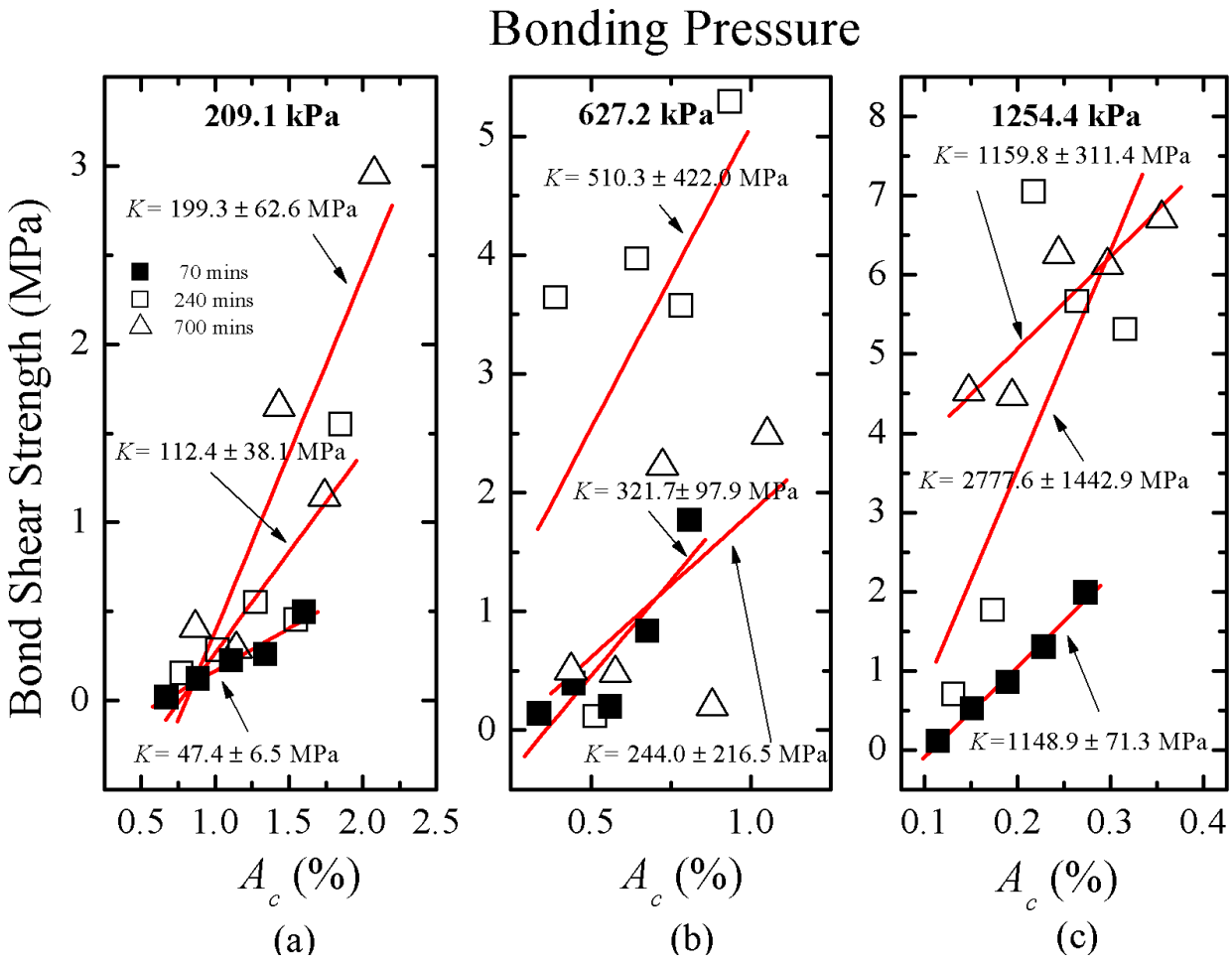

Fig. 8 Empirical determination of K by fitting the measured shear strengths to the calculated true contact areas from the model. K is found to be in the range of 42 MPa-2800 MPa as bonding load increases. Bonding loads of (a) 209.1 kPa, (b) 627.2 kPa, and (c) 1254.4 kPa.

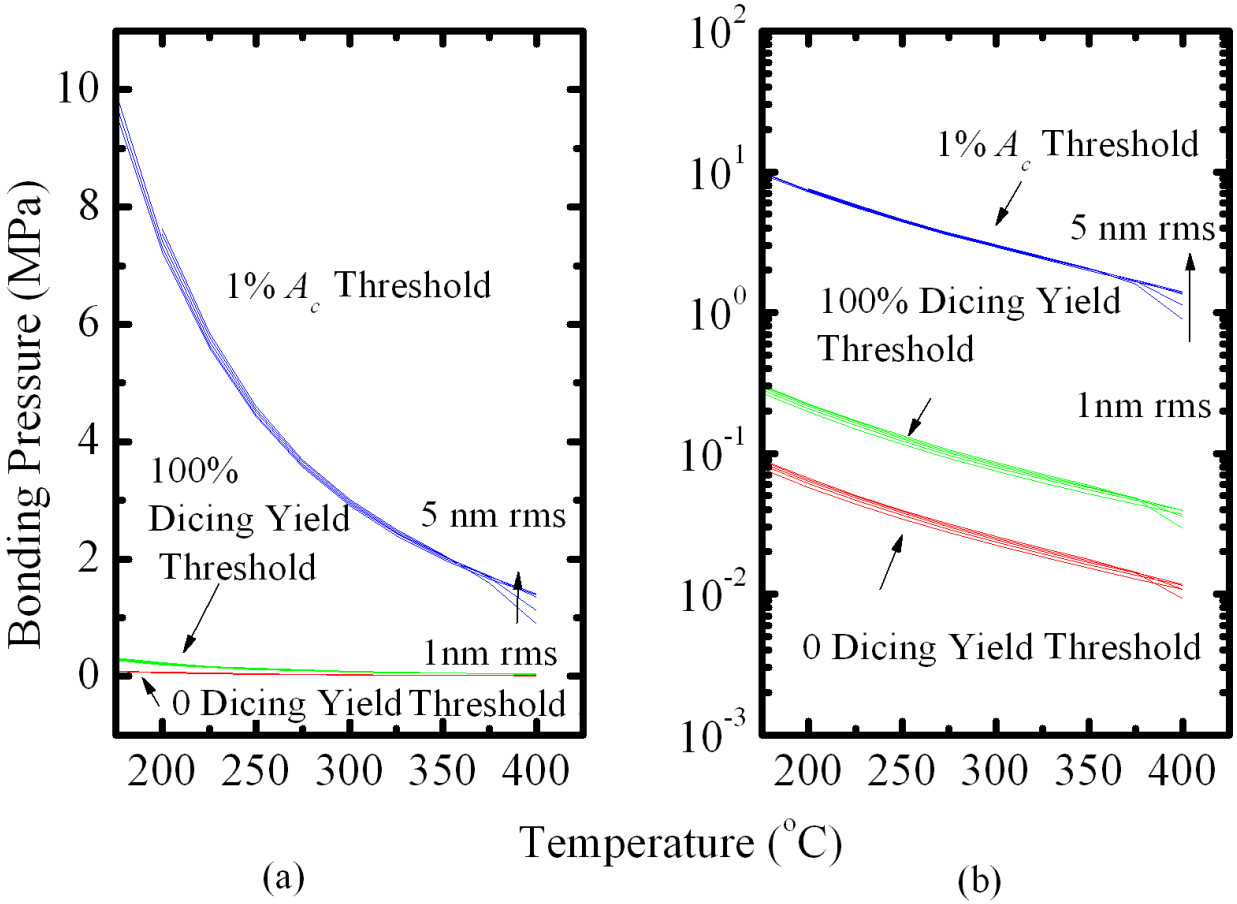

Fig. 9 True contact area bonding map for 1h of bonding for different surface roughness. (a) Linear scale. (b) Log scale.